Temperature Dependence of the Structure of the Substrate and Active Site of the *Thermus thermophilus* Chorismate Mutase E·S Complex†

Xiaohua Zhang and Thomas C. Bruice*

Department of Chemistry and Biochemistry, University of California, Santa Barbara, California 93106

Received March 2, 2006; Revised Manuscript Received April 28, 2006

ABSTRACT: Molecular dynamics (MD) simulations of *Thermus thermophilus* chorismate mutase substrate complex (TtCM·S) have been carried out at 298 K, 333 K, and the temperature of optimum activity: 343 K. The enzyme exists as trimeric subunits with active sites shared between two neighboring subunits. Two features distinguish intersubunit linkages of the thermophilic and mesophilic enzyme *Bacillus subtilis* chorismate mutase substrate complex (BsCM·S): (i) electrostatic interactions by intersubunit ion pairs (Arg3-Glu40*/41, Arg76-Glu51* and Arg69*-Asp101, residues labeled with an asterisk are from the neighboring subunit) in the TtCM·S are not present in the structure of the BsCM·S; and (ii) replacement of polar residues with short and nonpolar residues in the interstices of the TtCM·S tighten the intersubunit hydrophobic interactions compared to BsCM·S. Concerning the active site, electrostatic interactions of the critically placed Arg6 and Arg63* with the two carboxylates of chorismate place the latter in a reactive conformation to spontaneously undergo a Claisen rearrangement. The optimum geometry at the active site has the CZ atoms of the two arginines 11 Å apart. With a decrease in temperature, Arg63* moves toward Arg6 and the average conformation structure of chorismate moves further away from the reactive ground state conformation. This movement is due to the decrease in distance separating the electrostatic (in the main) and hydrophobic interacting pairs holding the two subunits together.

Over past decades, numerous thermophilic enzymes have been discovered (*1*). Both experimental (*2*−*8*) and theoretical (*9*−*14*) studies have been performed to gain understanding of various features that allow enzymes to survive and operate at high temperatures. Much attention has been given to understanding enzyme stability and activity (*15*−*19*). This report on the E·S complex of *Thermus thermophilus* chorismate mutase (TtCM[1]) and a recent study (*20*) of the E·S complex of the *Sulfolobus sulfataricus* thermophilic indole-3-glycerol phosphate synthase (IGP) are the first studies that elucidate the dependence of the E·S active site structure on temperature.

The chorismate to prephenate enzymatic reaction (Scheme 1) has been investigated intensively via various theoretical methods (*21*−*25*) on the basis that it is a one-substrate enzyme reaction which does not involve the formation of a covalent intermediate. These features simplify the determination of the ground state structure contribution to the enzymatic activity (*26*). A recent study (*27*) dealt with QM/MM investigations of the mechanism of the thermophilic enzyme TtCM at the optimum temperature (343 K). The mechanism of TtCM was found to be exactly that shown previously for the *Escherichia coli* (*28*) and *Bacillus subtilis* (*29*) enzymes at ambient temperature.

Scheme 1

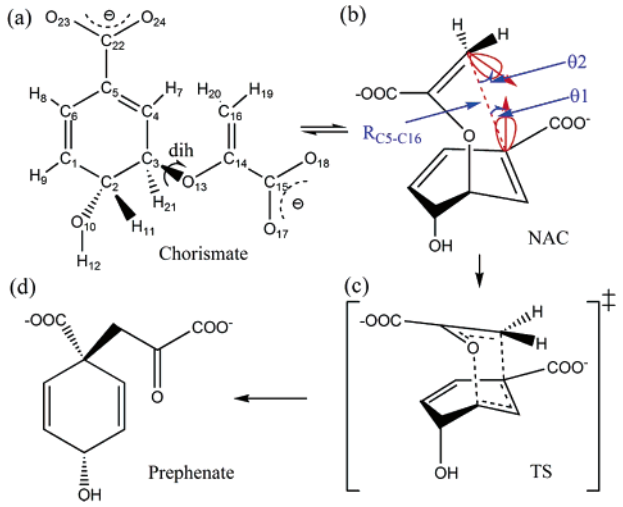

Several thermophilic chorismate mutases have been examined in recent years. These include *Thermus thermophilus* chorismate mutase by Tahirov and co-workers (*30*), *Methanococcus jannaschii* chorismate mutase by Hilvert and co-workers (*31*), and *Clostridium thermocellum* chorismate mutase (PDB entry, 1xho) by Wang and co-workers (*32*). TtCM is a homotrimer consisting of three pseudo-α/*β* barrels. Three active sites are formed in the interstices between three subunits. Each active site is composed of the residues of two adjacent subunits (Figure 1). The residues in close vicinity to the chorismate substrate are Arg6, Glu77, Arg89, Tyr107, Leu114, and Arg115 from one subunit and Phe57*, Ala59*, Arg63*, Leu72*, and Leu73* from the other subunit.

† Supported by the National Institutes of Health Grant 5R37DK9174-41.

* To whom correspondence should be addressed. Tel: (805) 893-2044. Fax: (805) 893-2229. E-mail: tcbruice@chem.ucsb.edu.

[1] Abbreviations: TtCM, *Thermus thermophilus* chorismate mutase; BsCM, *Bacillus subtilis* chorismate mutase; MD, molecular dynamics.

10.1021/bi0604227 CCC: $33.50
Published on Web 06/27/2006

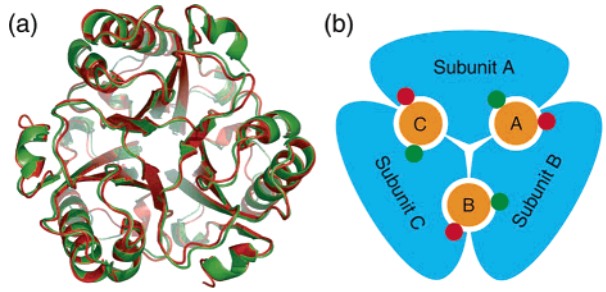

FIGURE 1: Chorismate mutase. (a) Overlap of TtCM (green) and BsCM (red) trimers using ribbon representation. (b) Model of the chorismate mutase trimer E·S. The substrates in the active sites are labeled by A, B, and C. The subunits are in blue, and substrates are in orange. The red dots designate Arg63*, and the green dots denote Arg6. The two arginines, Arg6 and Arg63* from adjacent subunits, hold the chorismate in the active site.

METHODS

Initial Structure Preparations. The initial TtCM·S structure was modified from an X-ray crystal structure of the F55S mutant (PDB entry, 1ODE; resolution, 1.65 Å) (*30*), so that the wild-type TtCM·S was created in a procedure described in the previous work (*27*). Chorismate conformations were docked into the active sites of the TtCM using SYBYL 6.8 (*33*). The initial structure for BsCM·S was taken from one of four trimers of the X-ray crystal structure (PDB ID, 2CHT; resolution, 2.2 Å) (*29*). The chorismate transition state analogues in the active sites were replaced by chorismates. The enzyme−substrate complexes were solvated using an orthorhombic water box with dimensions 72 Å × 71 Å × 63 Å, containing 8900 and 8315 TIP3P water molecules (*34*) for TtCM·S and BsCM·S, respectively. Water molecules within 2.8 Å of any non-hydrogen enzyme−substrate atoms were removed. To neutralize the net negative charges of the resulting systems of TtCM·S and BsCM·S, water molecules nearest to the negatively charged surface of the enzyme were replaced by sodium cations.

MD Simulations. The CHARMM27 force field was employed in the MD simulations (*35*). The force field for the chorismate was derived as described in previous work (*36*). The enzyme−substrate with water solvent and counterions was energy-minimized by the steepest descent (SD) and adopted basis Newton−Raphson (ABNR) methods. The Verlet Leapfrog integration was used to integrate the equations of motion with an integration time step of 1.5 fs (*37*). The SHAKE algorithm was applied to constrain all covalent bonds involving hydrogen (*38*). Periodic boundary conditions were applied in the simulations, and images were generated using the CRYSTAL facility of CHARMM employing orthorhombic symmetry. Electrostatic interactions were treated with the particle mesh Ewald (PME) method (*39*). PME calculations were performed using a real space cutoff of 9 Å with Lennard-Jones interactions truncated at the same distance. Harmonic constraints were added to both enzyme and substrates before the equilibrium phase and released steadily during the equilibrium. The system was gently heated from 50 K to the desired equilibrium temperature under constant pressure (1 atm). The system was maintained at the desired equilibrium temperature by coupling to a heat bath under constant pressure (1 atm) until the changes of the water box sizes were small. The subsequent simulations were carried out at constant volume and desired temperatures without constraints after equilibrium. MD simulation trajectories in NVT ensemble for TtCM·S were obtained at 298, 333, and 343 K during the dynamic runs, and at 303 and 500 K for BsCM·S. The simulation times were followed to 3 ns for each trajectory.

RESULTS

RMSF Calculation. The theoretical root-mean-square fluctuations (RMSFs) were obtained from MD simulations in water solvent at three different temperatures (298, 333, and 343 K). The experimental RMSF were calculated from the *B*-factor of enzyme crystallography as shown in the Supporting Information. The theoretical and experimental RMSF of C_α atoms of the TtCM residue are compared (Supporting Information, Figure S2). The corresponding positional fluctuations from the MD simulation are in good agreement with those obtained by X-ray crystallography. Regions which show flexibility in the crystal structure are well reproduced in the MD simulation trajectory.

Active Site. The average structures of the thermophilic E·S complex at three different temperatures (298, 333, and 343 K) were obtained from the MD simulations. A snapshot of the most important features of the active site of the TtCM E·S complex at 343 K is shown in Figure 2. These features are now described.

Arg6 and Arg63.* Arg6 is rigidly fixed at the active site in a subunit while Arg63* is inserted into the active site from an adjacent subunit. At the optimal temperature, Arg63* and Arg6 hold the chorismate in a reactive conformation (Figure 2) through hydrogen bonds with the two chorismate carboxylates. The hydrogen bonding (hydrogen of Arg6 and Arg63* guanidinium groups and chorismate carboxylate oxygen) distances range from 1.6 to 1.8 Å at various temperatures. Thus, the distances between the two arginines and chorismate carboxylates change only marginally with changes in temperature. However, the distance between Arg6 and Arg63* decreases as the temperature decreases (Figure 3). The distance between the CZ atoms in these two arginines changes from 11.0 to 8.1 Å when the temperature decreases from the optimal (343 K) to room temperature (298 K). As the temperature decreases, the two arginines steer the two carboxylates together so that the chorismate reacting atoms, C16 and C5, move away from each other (Figure 3).

Leu114 and Ala59.* At optimum temperature, Leu114 and Ala59* are in van der Waals distance to the reacting atoms C5 and C16 of chorismate, respectively (Figure 2). At 343 K, Leu114 and Ala59* act as "bookends" to prevent chorismate C5 and C16 atoms from moving away from their close positioning in the reactive conformer at the TtCM active site. The distances between the C_β atoms of Leu114 and Ala59* are 10.6, 11.7, and 11.9 Å at 298, 333, and 343 K, respectively. Leu114 is in the highly flexible C-terminus, and Ala59* is at the head of the H2 pattern (Figure 4) buried in the hydrophobic core, which is rather rigid. The decrease in the distance between Leu114 and Ala59* with a decrease in temperature is due to the movement of the C-terminus, and is associated with deformation at the active site. The movement of Leu114 toward Ala59* is much the same as movement of Arg63* toward Arg6 which leads the distortion of active site.

Arg89 and Glu77. Arg89 and Glu77 are in the same subunit as Arg6. The average distance between the NH1

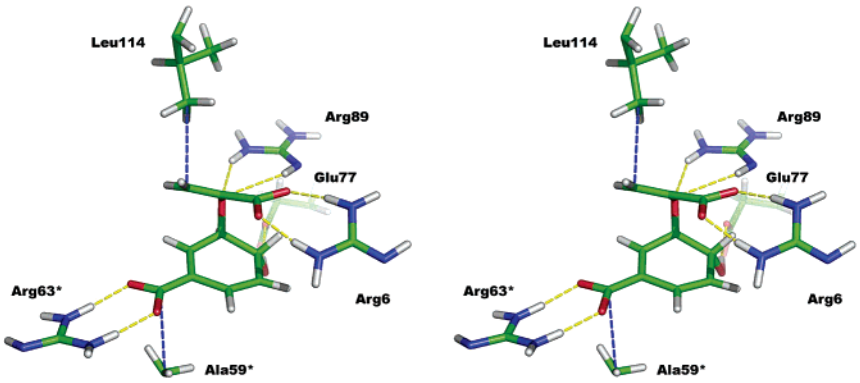

FIGURE 2: Stereoplot of a snapshot of the TtCM·S active site at 343 K. Only the critical residues in the active site are shown. The yellow dashed lines are hydrogen bonds, and the blue ones are van der Waals interactions.

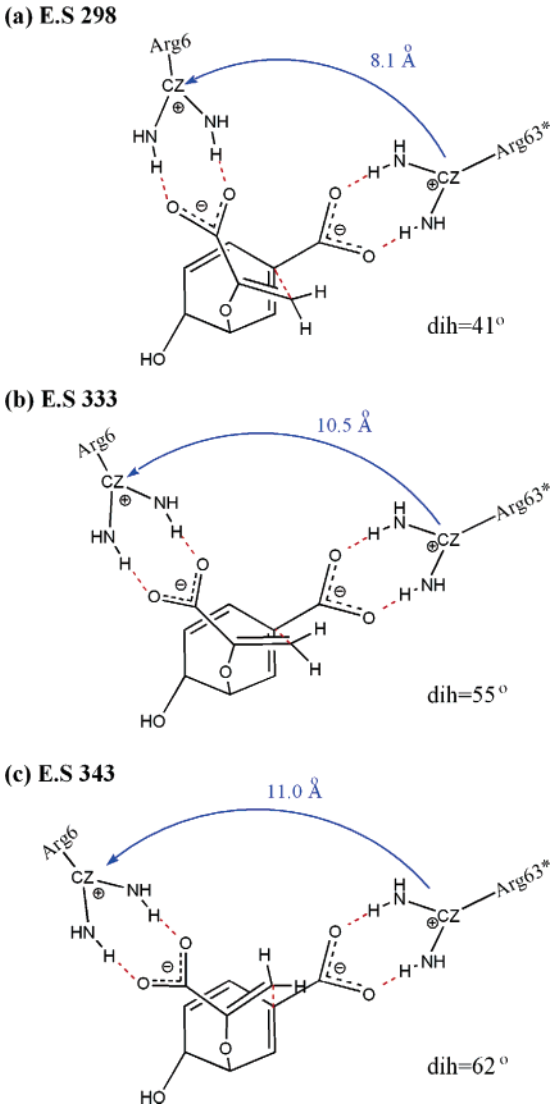

FIGURE 3: The two arginines hold the chorismate. Crucial distance between Arg6 and Arg63* controls the conformation of the chorismate.

nitrogen of the Arg89 guanidinium group and the ether oxygen O13 of chorismate varies little with temperature: 2.89, 2.85, and 2.92 Å at 298, 333, and 343 K, respectively. This lack of temperature dependence is related to Arg89 belonging to the pattern S4 (Figure 4), a structure with little motion in the MD simulations. The interaction of Glu77-COOH and the hydroxyl group of chorismate has average

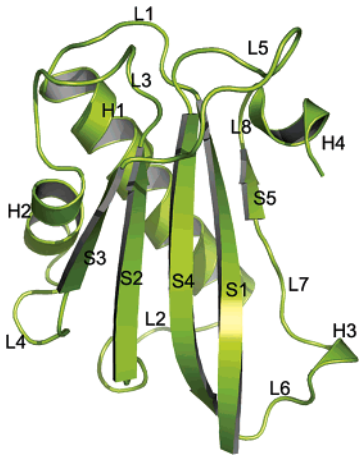

FIGURE 4: Subunit A of the TtCM trimer. S stands for sheet, H for helix, and L for loop. The subunit is composed of S1 (1−9), L1 (10−16), H1 (17−33), L2 (34−42), S2 (43−48), L3 (49−57), H2 (58−65), L4 (66−71), S3 (72−76), L5 (77−86), S4 (87−96), L6 (97−99), H3 (100−102), L7 (103−105), S5 (106−108), L8 (109−110), and H4 (111−115).

OE2−O10 distances of 3.11, 3.47, and 3.51 Å at 298, 333, and 343 K, respectively. Thus, the distance between Glu77-COOH and the hydroxyl oxygen decreases as temperature decreases from the optimum. This is due to the carboxylic acid oxygen being pushed by the movement of Arg63* as the temperature decreases. Thus, the chorismate hydroxyl oxygen moves away from Glu77-COOH at lower temperatures.

Average chorismate conformation structures are the average of the Boltzmann distribution of chorismate conformers at the active site in TtCM·S at given temperatures as determined by MD simulations. At 343 K (the temperature for optimum activity), the Boltzmann distribution is primarily composed of reactive conformers—near attack conformers (NACs, Scheme 1). NACs become fewer in Boltzmann distributions as the temperature decreases. A description of average chorismate conformations follows (Figure 5). The average distances between C5 and C16 at 298, 333, and 343 K are 4.04, 3.65, and 3.48 Å. The average angles of the C16 approaching the C5 π-orbital are 54°, 33°, and 28°, and the average angles of the C5 approaching the C16 π-orbital are 36°, 27°, and 26°.

Ion Pairs. Electrostatic interactions of ion pair networks are established on the surface and in the interstice of subunits. Thus, they can be divided into two categories: inter- and

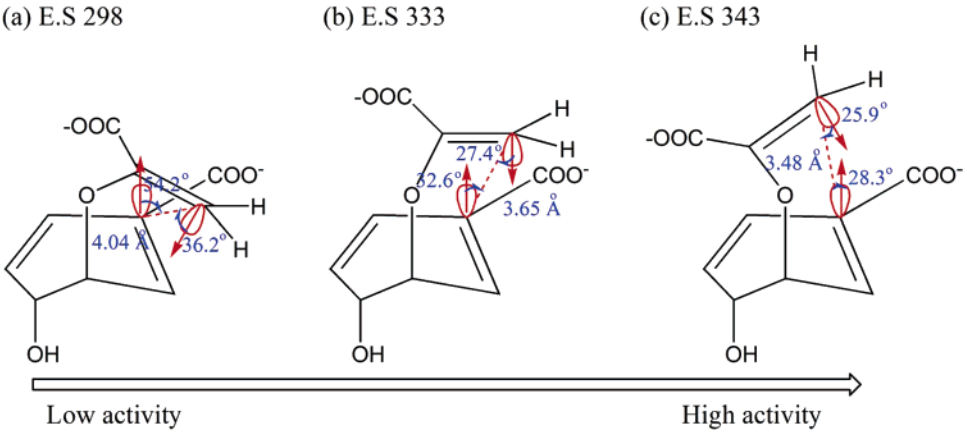

FIGURE 5: The average of the Boltzmann distribution of chorismate conformers at the active site of TtCM·S. As the temperature decreases, the reactive conformer represent a smaller portion of the Boltzmann distributions.

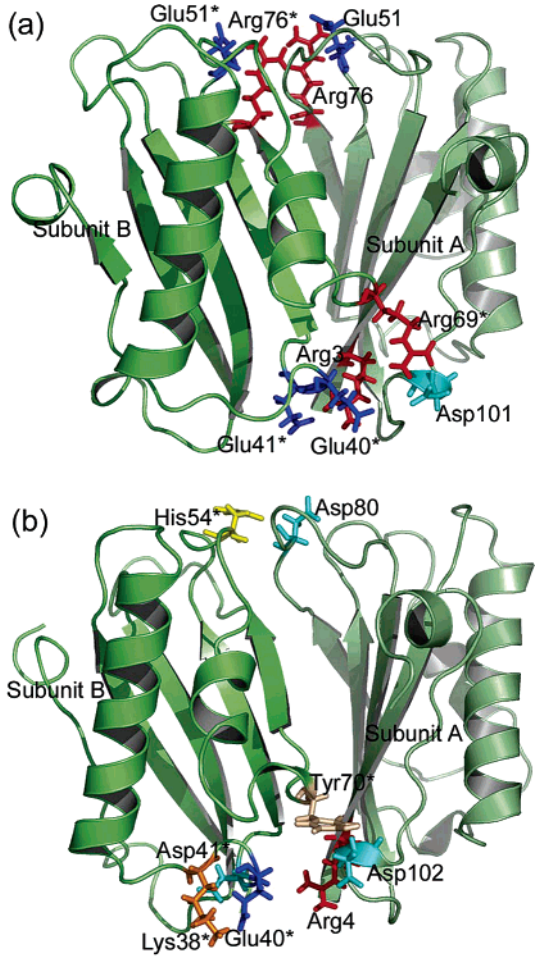

FIGURE 6: The intersubunit ion pairs for the TtCM·S (a) and BsCM·S (b). The snapshots for TtCM·S and BsCM·S are taken from the stable MD simulation trajectory at 343 and 303 K, respectively. The residues from subunit B are labeled by an asterisk.

intrasubunit ion pairs. The description of intrasubunit ion pairs can be found in the Supporting Information.

Intersubunit ion pairs in TtCM·S are formed between Arg3 and Glu40*/Glu41*, Arg69* and Asp101, and Arg76 and Glu51* (Figure 6a). However, only one intersubunit ion pair, His53*−Asp79, is present in the BsCM·S (Figure 6b). The correlated coefficients (C_{ij}) between residues reveal the long-range motion of the enzyme (Supporting Information). Positively correlated residues move in the same direction,

Table 1: The Correlated Coefficients of Residues for the Intersubunit Interactions[a]

	A−B	B−C	C−A
	TtCM		
Arg3−Glu40*	0.85	0.84	0.85
Arg3−Glu41*	0.81	0.80	0.82
Asp101−Arg69*	0.78	0.85	0.79
Arg76−Glu51*	0.74	0.80	0.72
Glu51−Arg76*	0.80	0.78	0.81
	BsCM		
Arg4−Glu40*	0.69	0.70	0.76
Arg4−Asp41*	0.70	0.70	0.78
Asp80−His54*	0.82	0.82	0.83

[a] Residues labeled by asterisk are from neighboring subunit.

Table 2: The Average Distances (Å) of C_ξ Atoms for Intersubunit Interactions[a]

	A−B	B−C	C−A
	TtCM		
Arg3(CZ)−Glu40*(CD)	6.26 ± 0.90	7.52 ± 0.81	6.31 ± 1.17
Arg3(CZ)−Glu41*(CD)	8.36 ± 1.42	7.63 ± 2.15	8.28 ± 0.96
Arg76(CZ)−Glu51*(CD)	12.47 ± 2.47	6.97 ± 0.72	10.90 ± 1.41
Glu51(CD)−Arg76*(CZ)	6.98 ± 1.92	7.61 ± 1.16	4.83 ± 0.61
Asp101(CG)−Arg69*(CZ)	5.20 ± 1.10	5.78 ± 0.93	5.42 ± 1.32
	BsCM		
Arg4(CZ)−Glu40*(CD)	8.18 ± 0.71	8.60 ± 0.87	8.61 ± 0.53
Arg4(CZ)−Asp41*(CG)	8.08 ± 0.86	8.94 ± 0.94	7.96 ± 0.51
Asp80(CG)−His54*(CE1)	6.00 ± 1.03	5.86 ± 0.96	6.39 ± 1.03

[a] The C_ξ atom is the carbon at the end of the side chain.

whereas (negatively) anticorrelated residues move in the opposite direction. A completely correlated or anticorrelated motion ($C_{ij} = 1$ or $C_{ij} = -1$) denotes that the motions have the same or opposite phase and period. The average correlated coefficients between Arg3 and Glu40*/41 in TtCM·S are 0.85 and 0.81 (Table 1) and between Arg4 and Glu40*/Asp41 in BsCM·S are 0.72 and 0.73. The average distance (Table 2) between Arg3(CZ) and Glu40*(CG) in the TtCM·S is 6.70 Å, while that between Arg4(CZ) and Glu40*(CG) in the BsCM·S is much longer (8.46 Å). Thus, observed from both correlated coefficients and distances apart of the ion pair, the Arg4−Glu40* ion pair in BsCM·S is much weaker than the Arg3−Glu40* in TtCM·S. This is due to the competing formation of the Lys37−Glu40* pair. Arg69*−Asp101 in TtCM·S is replaced by Tyr70*−Asp102 in BsCM·S. The replacement of an ion pair by a non-ion

pair severely weakens the intersubunit electrostatic interactions. Thus, the overall intersubunit electrostatic interactions of BsCM·S (303 K) are much weaker than that of TtCM·S (343 K).

DISCUSSION

The intersubunit electrostatic and hydrophobic interactions, which stabilize the TtCM trimer (see the Supporting Information), are also responsible for loss of activity at lower temperatures. The distances between electrostatic and hydrophobic pairs decrease as temperature decreases. Thus the TtCM·S trimer is compressed as the temperature decreases. One of the most pivotal consequences of the pushing together of the TtCM·S trimeric structure is Arg63* moving toward Arg6 (residues labeled with an asterisk are from the neighboring subunit). The hydrogen bonding of Arg6 and Arg63* with the two carboxylate functional groups of chorismate, at optimum temperature, creates the active conformation which allows the chorismate → prephenate rearrangement (Figure 2). As Arg63* moves toward Arg6 with the lowering of temperature, there is a forced rotation around the chorismate dihedral angle dih (Scheme 1: C4−C3−O13−C14). The average value of dih changes from 62° to 41° with a decrease in temperature from 343 to 298 K (Figure 3). Karplus et al. determined that the chair conformations with dih = 60−70° are the major and most reactive conformers in the BsCM active site by generating the PMF profile along the dih angle (*24*). Our previous thermodynamic integration results of BsCM have also shown that the dih = 60−70° are associated with the lowest free energy for chorismate → prephenate reaction in the BsCM·S and *E. coli* enzyme (*21*). The same is true for the TtCM enzymatic reaction. The average chorismate conformation at the optimum temperature of 343 K is characterized by a dih of 62°.

The H2 helix pattern, which contains Arg63* and connects to both L3 and L4 (Figure 4), buries its head (residue positions 58−61) into the hydrophobic core and exposes its tail (residue positions 62−65) to the solvent. Identified by normal-mode analysis (NMA, Supporting Information), collective motions of the H2 tail become nontrivial as the corresponding frequency of the motions increases. This indicates that the H2 tail is extended at higher temperature. In other words, the H2 tail will be contracted as temperature decreases from the optimal temperature. Arg6 is attached to the pattern S1, which is quite stable as has been confirmed by RMSF of TtCM·S C_α atoms and by NMA. Therefore, Arg63* is moved toward Arg6, resulting in the turning away of reacting atoms C5 and C16 of the chorismate. The average chorismate conformation at lower temperatures is less reactive (Figure 5).

As shown in the Supporting Information, the collective motions for the active sites at low frequencies, obtained from NMA, are barely significant. The structure of the thermophilic enzyme trimer is rigid. This suggests that thermal motion cannot be involved in the mechanism of chorismate mutase enzymes and agrees with the role of these enzymes being to create reactive substrate conformers, which proceed to TtCM·TS with little help from the enzyme (*21*−*23*).

The MD simulation of the BsCM·S has shown that the distance of CZ atoms in the two arginines, Arg6 and Arg63* (10.8 Å), is larger than the distance of the CZ atoms in Arg7 and Arg63* of TtCM·S (8.1 Å) at room temperature, but similar to that for TtCM·S (11.0 Å) at their optimal growth temperatures (298 and 343 K for BsCM and TtCM, respectively). The similarity of the separating distances of the two arginines for TtCM·S and BsCM·S at their optimal conditions indicates that the two enzymes have equivalent ability in creating the reactive ground state conformer of the substrate under their optimal conditions. This finding is in agreement with the experimental observation that the catalytic constant (52 s^{-1} at 343 K) for TtCM (*30*) is similar to that of BsCM (50 s^{-1} at 303 K) (*40*, *41*).

CONCLUSION

The family of chorismate mutase enzymes shares a common E·S active site. The chorismate is held in the active site by two arginines which are hydrogen bonded to the two chorismate carboxylates. This arrangement stabilizes the reactive conformation of the substrate which undergoes Claisen rearrangement to prephenate. The stabilization is also helped by two hydrophobic side chains which are in van der Waals distance from the reacting chorismate carbons, much like "bookends". Thermophilic enzymes evolve such that their active site structures are at perfection to preferentially bind the substrate as a reactive conformer at a given elevated temperature.

The MD simulations of *T. thermophilus* chorismate mutase (TtCM) E·S complex in solvent water have been performed at various temperatures. TtCM is a trimeric enzyme with three homologous subunits. As the temperature is lowered, distances of electrostatic and hydrophobic interactions decrease. The interstices between TtCM subunits are compressed by the tightening of intersubunit interactions, leading to a pushing of Arg63* in one subunit toward Arg6 in a neighboring subunit. This results in a distorted active site so that the bound substrate is less often in a reactive conformation. With a decrease in temperature, the reacting chorismate atoms (C5 and C16) become farther apart due to changes in the dihedral angle of the diaxial chorismate structure. Thus, the enzyme activity dwindles. This is very much the same as seen when the reaction temperature of the *S. sulfataricus* thermophilic indole-3-glycerol phosphate synthase (IGP) E·S complex (*20*) is decreased from the optimum temperature of 385 K (*42*). In the reaction of IGP·S, as in the reaction of TtCM·S, with a drop in temperature electrostatic bonds between enzyme and substrate diminish in length, and a substrate dihedral angle critical to the formation of the indole ring increases with a decrease in temperature.

ACKNOWLEDGMENT

We express appreciation to the National Institutes of Health (Grant 5R37DK9174-41) and the National Partnership for Advanced Computational Infrastructure for its generous allocation of computational resources at DataStar in the University of California at San Diego Supercomputing Center (SDSC). The authors thank referees for valuable comments.

SUPPORTING INFORMATION AVAILABLE

The Stability of Intersubunit Interactions for the *Thermus thermophilus* Chorismate Mutase is available free of charge via the Internet at http://pubs.acs.org.

REFERENCES

1. Vieille, C., and Zeikus, G. J. (2001) Hyperthermophilic enzymes: Sources, uses, and molecular mechanisms for thermostability, *Microbiol. Mol. Biol. Rev. 65*, 1−43.
2. Kim, H. S., Damo, S. M., Lee, S. Y., Wemmer, D., and Klinman, J. P. (2005) Structure and hydride transfer mechanism of a moderate thermophilic dihydrofolate reductase from Bacillus stearothermophilus and comparison to its mesophilic and hyperthermophilic homologues, *Biochemistry 44*, 11428−11439.
3. Liang, Z. X., Lee, T., Resing, K. A., Ahn, N. G., and Klinman, J. P. (2004) Thermal-activated protein mobility and its correlation with catalysis in thermophilic alcohol dehydrogenase, *Proc. Natl. Acad. Sci. U.S.A. 101*, 9556−9561.
4. D'Amico, S., Marx, J. C., Gerday, C., and Feller, G. (2003) Activity-stability relationships in extremophilic enzymes, *J. Biol. Chem. 278*, 7891−7896.
5. Wolf-Watz, M., Thai, V., Henzler-Wildman, K., Hadjipavlou, G., Eisenmesser, E. Z., and Kern, D. (2004) Linkage between dynamics and catalysis in a thermophilic-mesophilic enzyme pair, *Nat. Struct. Mol. Biol. 11*, 945−949.
6. Zhang, Z. L., Tsujimura, M., Akutsu, J., Sasaki, M., Tajima, H., and Kawarabayasi, Y. (2005) Identification of an extremely thermostable enzyme with dual sugar-1-phosphate nucleotidylyltransferase activities from an acidothermophilic archaeon, Sulfolobus tokodaii strain 7, *J. Biol. Chem. 280*, 9698−9705.
7. De Simone, G., Menchise, V., Manco, G., Mandrich, L., Sorrentino, N., Lang, D., Rossi, M., and Pedone, C. (2001) The crystal structure of a hyper-thermophilic carboxylesterase from the archaeon Archaeoglobus fulgidus, *J. Mol. Biol. 314*, 507−518.
8. Viard, T., Lamour, V., Duguet, M., and de la Tour, C. B. (2001) Hyperthermophilic topoisomerase I from Thermotoga maritima. A very efficient enzyme that functions independently of zinc binding, *J. Biol. Chem. 276*, 46495−46503.
9. Tidor, B., and Karplus, M. (1991) Simulation Analysis of the Stability Mutant R96h of T4 Lysozyme, *Biochemistry 30*, 3217−3228.
10. Lazaridis, T., Lee, I., and Karplus, M. (1997) Dynamics and unfolding pathways of a hyperthermophilic and a mesophilic rubredoxin, *Protein Sci. 6*, 2589−2605.
11. Hartsough, D. S., and Merz, K. M. (1993) Protein Dynamics and Solvation in Aqueous and Nonaqueous Environments, *J. Am. Chem. Soc. 115*, 6529−6537.
12. Levy, Y., Caflisch, A., Onuchic, J. N., and Wolynes, P. G. (2004) The folding and dimerization of HIV-1 protease: Evidence for a stable monomer from simulations, *J. Mol. Biol. 340*, 67−79.
13. Wang, W., and Kollman, P. A. (2000) Free energy calculations on dimer stability of the HIV protease using molecular dynamics and a continuum solvent model, *J. Mol. Biol. 303*, 567−582.
14. Wintrode, P. L., Zhang, D. Q., Vaidehi, N., Arnold, F. H., and Goddard, W. A. (2003) Protein dynamics in a family of laboratory evolved thermophilic enzymes, *J. Mol. Biol. 327*, 745−757.
15. Mandrich, L., Merone, L., Pezzullo, M., Cipolla, L., Nicotra, F., Rossi, M., and Manco, G. (2005) Role of the N terminus in enzyme activity, stability and specificity in thermophilic esterases belonging to the HSL family, *J. Mol. Biol. 345*, 501−512.
16. Collins, T., Meuwis, M. A., Gerday, C., and Feller, G. (2003) Activity, stability and flexibility in Glycosidases adapted to extreme thermal environments, *J. Mol. Biol. 328*, 419−428.
17. Bogin, O., Levin, I., Hacham, Y., Tel-Or, S., Peretz, M., Frolow, F., and Burstein, Y. (2002) Structural basis for the enhanced thermal stability of alcohol dehydrogenase mutants from the mesophilic bacterium Clostridium beijerinckii: contribution of salt bridging, *Protein Sci. 11*, 2561−2574.
18. Dalhus, B., et al. (2002) Structural basis for thermophilic protein stability: Structures of thermophilic and mesophilic malate dehydrogenases, *J. Mol. Biol. 318*, 707−721.
19. Fitter, J., Herrmann, R., Dencher, N. A., Blume, A., and Hauss, T. (2001) Activity and stability of a thermostable alpha-amylase compared to its mesophilic homologue: Mechanisms of thermal adaptation, *Biochemistry 40*, 10723−10731.
20. Mazumder-Shivakumar, D., Kahn, K., and Bruice, T. C. (2004) Computational study of the ground state of thermophilic indole glycerol phosphate synthase: Structural alterations at the active site with temperature, *J. Am. Chem. Soc. 126*, 5936−5937.
21. Hur, S., and Bruice, T. C. (2003) The near attack conformation approach to the study of the chorismate to prephenate reaction, *Proc. Natl. Acad. Sci. U.S.A. 100*, 12015−12020.
22. Hur, S., and Bruice, T. C. (2003) Comparison of formation of reactive conformers (NACs) for the Claisen rearrangement of chorismate to prephenate in water and in the E-coli mutase: The efficiency of the enzyme catalysis, *J. Am. Chem. Soc. 125*, 5964−5972.
23. Zhang, X. D., Zhang, X. H., and Bruice, T. C. (2005) A definitive mechanism for chorismate mutase, *Biochemistry 44*, 10443−10448.
24. Guo, H., Cui, Q., Lipscomb, W. N., and Karplus, M. (2003) Understanding the role of active-site residues in chorismate mutase catalysis from molecular-dynamics simulations, *Angew. Chem., Int. Ed. 42*, 1508−1511.
25. Strajbl, M., Shurki, A., Kato, M., and Warshel, A. (2003) Apparent NAC effect in chorismate mutase reflects electrostatic transition state stabilization, *J. Am. Chem. Soc. 125*, 10228−10237.
26. Bruice, T. C. (2002) A view at the millennium: The efficiency of enzymatic catalysis, *Acc. Chem. Res. 35*, 139−148.
27. Zhang, X.-H., and Bruice, T. C. (2005) The proficiency of a thermophilic chorismate mutase enzyme is solely through an entropic advantage in the enzyme reaction, *Proc. Natl. Acad. Sci. U.S.A. 102*, 18356−18360.
28. Lee, A. Y., Karplus, P. A., Ganem, B., and Clardy, J. (1995) Atomic-Structure of the Buried Catalytic Pocket of Escherichia-Coli Chorismate Mutase, *J. Am. Chem. Soc. 117*, 3627−3628.
29. Chook, Y. M., Ke, H. M., and Lipscomb, W. N. (1993) Crystal-Structures of the Monofunctional Chorismate Mutase from Bacillus-Subtilis and Its Complex with a Transition-State Analog, *Proc. Natl. Acad. Sci. U.S.A. 90*, 8600−8603.
30. Helmstaedt, K., Heinrich, G., Merkl, R., and Braus, G. H. (2004) Chorismate mutase of Thermus thermophilus is a monofunctional AroH class enzyme inhibited by tyrosine, *Arch. Microbiol. 181*, 195−203.
31. MacBeath, G., Kast, P., and Hilvert, D. (1998) A small, thermostable, and monofunctional chorismate mutase from the archeon Methanococcus jannaschii, *Biochemistry 37*, 10062−10073.
32. Xu, H., et al. (2005) Away from the edge II: in-house Se-SAS phasing with chromium radiation, *Acta Crystallogr., Sect. D 61*, 960−966.
33. SYBYL. 6.8, Tripos Inc., St. Louis, MO 63144.
34. Jorgensen, W. L., Chandrasekhar, J., Madura, J. D., Impey, R. W., and Klein, M. L. (1983) Comparison of Simple Potential Functions for Simulating Liquid Water, *J. Chem. Phys. 79*, 926−935.
35. Brooks, B. R., Bruccoleri, R. E., Olafson, B. D., States, D. J., Swaminathan, S., and Karplus, M. (1983) Charmm—a Program for Macromolecular Energy, Minimization, and Dynamics Calculations, *J. Comput. Chem. 4*, 187−217.
36. Hur, S., and Bruice, T. C. (2002) The mechanism of catalysis of the chorismate to prephenate reaction by the Escherichia coli mutase enzyme, *Proc. Natl. Acad. Sci. U.S.A. 99*, 1176−1181.
37. Verlet, L. (1967) Computer Experiments on Classical Fluids.I. Thermodynamical Properties of Lennard-Jones Molecules, *Phys. Rev. 159*, 98−103.
38. Ryckaert, J. P., Ciccotti, G., and Berendsen, H. J. C. (1977) Numerical-Integration of Cartesian Equations of Motion of a System with Constraints—Molecular-Dynamics of N-Alkanes, *J. Comput. Phys. 23*, 327−341.
39. Darden, T., York, D., and Pedersen, L. (1993) Particle Mesh Ewald—an N.Log(N) Method for Ewald Sums in Large Systems, *J. Chem. Phys. 98*, 10089−10092.
40. Gray, J. V., Eren, D., and Knowles, J. R. (1990) Monofunctional Chorismate Mutase from Bacillus-Subtilis—Kinetic and C-13 Nmr-Studies on the Interactions of the Enzyme with Its Ligands, *Biochemistry 29*, 8872−8878.
41. Mattei, P., Kast, P., and Hilvert, D. (1999) Bacillus subtilis chorismate mutase is partially diffusion-controlled, *Eur. J. Biochem. 261*, 25−32.
42. Merz, A., Yee, M. C., Szadkowski, H., Pappenberger, G., Crameri, A., Stemmer, W. P. C., Yanofsky, C., and Kirschner, K. (2000) Improving the catalytic activity of a thermophilic enzyme at low temperatures, *Biochemistry 39*, 880−889.

BI0604227